Eur Biophys J (2004) 33: 535–542
DOI 10.1007/s00249-004-0394-3

ARTICLE

Monika Krasowska · Zbigniew J. Grzywna
Maria E. Mycielska · Mustafa B. A. Djamgoz

Patterning of endocytic vesicles and its control by voltage-gated Na^+ channel activity in rat prostate cancer cells: fractal analyses

Received: 10 April 2003 / Revised: 2 June 2003 / Accepted: 23 January 2004 / Published online: 16 March 2004

Abstract Fractal methods were used to analyze quantitative differences in secretory membrane activities of two rat prostate cancer cell lines (Mat-LyLu and AT-2) of strong and weak metastatic potential, respectively. Each cell's endocytic activity was determined by horseradish peroxidase uptake. Digital images of the patterns of vesicular staining were evaluated by multifractal analyses: generalized fractal dimension (D_q) and its Legendre transform $f(\alpha)$, as well as partitioned iterated function system – semifractal (PIFS-SF) analysis. These approaches revealed consistently that, under control conditions, all multifractal parameters and PIFS-SF codes determined had values greater for Mat-LyLu compared with AT-2 cells. This would agree generally with the endocytic/vesicular activity of the strongly metastatic Mat-LyLu cells being more developed than the corresponding weakly metastatic AT-2 cells. All the parameters studied were sensitive to tetrodotoxin (TTX) pre-treatment of the cells, which blocked voltage-gated Na^+ channels (VGSCs). Some of the parameters had a "simple" dependence on VGSC activity, whereby pre-treatment with TTX reduced the values for the MAT-LyLu cells and eliminated the differences between the two cell lines. For other parameters, however, there was a "complex" dependence on VGSC activity. The possible physical/physiological meaning of the mathematical parameters studied and the nature of involvement of VGSC activity in control of endocytosis/secretion are discussed.

Keywords Endocytosis · Fractal · Metastasis · Tetrodotoxin · Voltage-gated sodium channel

M. Krasowska · M. E. Mycielska · M. B. A. Djamgoz (✉)
Neuroscience Solutions to Cancer Research Group,
Department of Biological Sciences,
Imperial College London,
Sir Alexander Fleming Building,
South Kensington Campus, London,
SW7 2AZ, UK
E-mail: m.djamgoz@imperial.ac.uk
Tel.: +44-207-5945370
Fax: +44-207-5842056

M. Krasowska · Z. J. Grzywna
Section of Physics and Applied Mathematics,
Department of Physical Chemistry and Polymer Technology,
Silesian University of Technology,
Strzody 9, 44-100 Gliwice, Poland

Introduction

The most significant aspect of cancer and the main cause of death in most cancer patients is metastasis. This is the overall process whereby cells escaping from a primary tumour enter circulation (lymph and/or blood), migrate around the body and become lodged at tissue-specific or non-specific sites where they re-proliferate to form secondary tumours (e.g. Liotta 1986; Bashyam 2002). Finally, the continued growth of the secondary (as well as the initial primary) tumours beyond some 0.5 mm depends on angiogenesis, i.e. formation of new blood vessels to ensure further supply of nutrients (Nicholson et al. 2001). An important cellular activity in metastasis, including angiogenesis, is secretion. Indeed, tumour cells secrete a variety of chemicals to control their proliferation, motility and survival (e.g. Evans et al. 1991). Such chemicals include growth factors, angiogenic signals and proteolytic enzymes (Kurbel et al. 1999; Lin et al. 2000). It is also known that malignant cancer cells depend on locally produced factors (including growth factors) which may be taken up through such processes as phagocytosis, pinocytosis and receptor-mediated endocytosis (Shtiegman and Yarden 2003). Endocytosis involves a variety of molecular mechanisms and is tightly regulated, both temporally and spatially (Conner and Schmid 2003; Grundelfinger et al. 2003).

At present, one of the most common cancers in the western world is that of the male prostate gland, and there is an urgent need to develop new diagnostic and therapeutic methods for its management (e.g. Foster et al. 1999). In a recent study, using horseradish peroxidase as a non-toxic intracellular tracer (Yang et al. 2000; Llorente et al. 2000), we have shown that rat

(''Dunning'') prostate cancer cells of strong versus weak metastatic potential differed in their endocytic membrane activity, hence probably secretion (Mycielska et al. 2003). Accordingly, the strongly metastatic Mat-LyLu cells were much more endocytic than the corresponding weakly metastatic AT-2 cells. Furthermore, endocytosis in Mat-LyLu cells was suppressed by tetrodotoxin (TTX)-induced blockage of the voltage-gated Na^+ channels (VGSCs), which were shown earlier to be expressed selectively in strongly metastatic cells (Grimes et al. 1995; Laniado et al. 1997).

Interestingly, the previous study (Mycielska et al. 2003) suggested in addition that as well as the quantity, these cells may also differ in the quality (i.e. pattern) of the vesicular uptake of HRP and that TTX also appeared to change the pattern of the labelling. In the present study, we have investigated this problem more rigorously by applying fractal methods (Grzywna and Stolarczyk 2002; Grzywna et al. 2003) to analyze the vesicular patterns generated by endocytic labelling of the two contrasting cell lines: Mat-LyLu cells, which metastasize in $>90\%$ of cases when injected into syngeneic rats, and AT-2 cells, which are metastatic only in $<10\%$ of cases; these cell lines were originally derived from the same tumour occurring spontaneously in a Copenhagen rat (Isaacs et al. 1986). Fractal analyses have already proven to be highly applicable to elucidation of a diverse variety of complex patterns such as neuronal dendritic trees (Djamgoz et al. 2001), trajectories of motile cells (Siwy et al. 2003), blood flow in relation to regional heterogeneity in lung (Bottino et al. 2001) and migraine (Latka et al. 2004), vascular networks (Vico et al. 1994), material surfaces (Almqvist 1996) and textures in static visual images (Turiel 2003).

Materials and methods

Labelling of endocytic vesicles by uptake of horseradish peroxidase

These experiments were carried out as described previously (Mycielska et al. 2003). Mat-LyLu and AT-2 cell lines were grown in supplemented RPMI medium in an incubator at 37 °C (Grimes et al. 1995). Uptake of horseradish peroxidase (HRP; Sigma type VI) was performed in Ringer solution in which the cells were first carefully rinsed. The cells were incubated with 0.5 mg/mL HRP for 40 min. In experiments testing the effect of VGSC blockage, 1 μM TTX was added to the incubation medium. The cells were then fixed in 4% paraformaldehyde in PBS and treated with diaminobenzidine (0.5 mg/mL) and hydrogen peroxide (0.01%) in 0.5 M Tris buffer, as described previously (Mycielska et al. 2003). Following dehydration, the cells were mounted in DPX. Labelled cells were imaged under a Zeiss Axiovert microscope using a ×100 oil immersion objective. The images were digitized using a CoolSNAP camera and measurements were made using Image-Pro Plus software (Media Cybernetics, Md., USA).

Analyses of the pattern of labelled vesicles

The patterns of staining were analyzed by means of established multifractal analyses (Djamgoz et al. 2001; Grzywna et al. 2001) as well as the relatively recently introduced ''partitioned iterated function system – semifractal'' (PIFS-SF) analysis (Grzywna and Stolarczyk 2002).

Theory

Multifractal analyses

These involved two approaches: (1) the generalized fractal dimension, D_q (''D_q spectrum'') and (2) the ''multifractal spectrum'', $f(\alpha)$ (Schroeder 1991; Djamgoz et al. 2001). Both methods generate an infinite set of numbers (dimensions) representing details (complexity, self-similarity, irregularity, etc.) of the structure being analyzed and both are needed for comprehensive understanding. The generalized fractal dimension is defined as follows:

$$D_q = \frac{1}{q-1}\lim_{\varepsilon\to 0}\frac{\ln\sum_{i=1}^{M(\varepsilon)} P_i^q}{\ln \varepsilon} \tag{1}$$

where q is a real number (dimension index), P_i is the probability of finding a point in the ith element of covering, ϵ is the width of the covering element, and $M(\epsilon)$ is the number of covering elements. From Eq. 1, it would follow that:

$$D_0 = \frac{1}{0-1}\lim_{\varepsilon\to 0}\frac{\ln\sum_{i=1}^{M(\varepsilon)} P_i^0}{\ln \varepsilon} = -\lim_{\varepsilon\to 0}\frac{\ln M(\varepsilon)}{\ln \varepsilon} = d_{\mathrm{F}} \tag{2}$$

and:

$$D_1 = -\lim_{\varepsilon\to 0}\frac{\sum_{i=1}^{M(\varepsilon)} P_i \ln P_i}{\ln \varepsilon} \tag{3}$$

and:

$$D_2 = \lim_{\varepsilon\to 0}\frac{\ln\sum_{i=1}^{M(\varepsilon)} P_i^2}{\ln \varepsilon} \tag{4}$$

Higher order fractals were not studied here. The fractal parameters were calculated using the most popular method of ''box counting'', since there was no circular regularity or special symmetry in the staining (Jelinek and Fernandez 1998; Djamgoz et al. 2001). The first box (of size ϵ) covered the whole object; next the object was embedded into a sequence of boxes of decreasing ϵ size, leading to boxes as small as possible, but still large enough for the probability to be defined (see Fig. 2).

The $f(\alpha)$ formalism (''multifractal spectrum'') is a Legendre transform of D_q and is defined as follows:

$$f(\alpha) = \alpha\tilde{q}(\alpha) - \tau_{\tilde{q}(\alpha)} \tag{5}$$

where:

$$\alpha = \frac{\partial \tau_q}{\partial \tilde{q}} \tag{6}$$

and:

$$\tau_q = (q-1)D_q = \lim_{\varepsilon\to 0}\frac{\ln\sum_{i=1}^{N(\varepsilon)} P_i^q}{\ln \varepsilon} \tag{7}$$

and $\tilde{q}$ is the dimension index. The full derivation of this transform was given previously (Djamgoz et al. 2001). $f(\alpha)$ is analogous to entropy, with α corresponding to the total energy (slope of straight line in the Legendre transform) (Stanley 1996).

The Legendre transform of D_q to $f(\alpha)$ basically ''shrinks'' the information-poor part of the D_q spectrum into a regular graph with a single maximum. Values of D_0, D_1 and D_2 (which have well-known physical meaning) are easily identifiable in the spectrum: the maximum of $f(\alpha)$ is equal to D_0; D_1 is an intercept of $f(\alpha)$ with the $f(\alpha)=\alpha$ line; and D_2 is an intercept of the $f(\alpha)=\alpha$ line with a tangent to $f(\alpha)$ which has a slope of 2. D_∞ and $D_{-\infty}$ depend on extreme

values of P_i and their difference describes the range of values that P_i takes (the span of the graph). They both make sense no matter what the values of $f(\alpha)$ for α_{min} and α_{max}. Thus, there is no need for extrapolation in cases where the roots are not present. Moreover, these values provide additional information about the multiplicity of P_{min} and P_{max}. D_q is difficult to analyze with respect to extreme values of P_i ($q \to \infty$ or $q \to -\infty$). On the other hand, $f(\alpha)$ shows clearly both the multiplicity of extreme values of P_i and the range of P_i. The domain of D_q is unbounded while the domain of $f(\alpha)$ is finite. Both D_q and $f(\alpha)$ show to what extent the P_i distribution deviates from uniform. Both are very sensitive (or even oversensitive) to defects in regular structures and are invariant to flipping, mirroring, rotation (by 90°, 180° and 270°) and shuffling of a given image.

PIFS-SF analysis

The basic idea of encoding an image in terms of transforms comes from the work on "iterated functions system" (Barnsley 1988). Since it is rather uncommon for any real object (image) to be composed of its own diminished copies, Jacquin (1993) enhanced the concept by allowing parts of the image to be contracted copies of different parts. In a further development, Grzywna and Stolarczyk (2002) adopted the notion of semifractals (Lasota and Myjak 1996) so that not all transforms would need to be contractive and some of them may be scale-preserving. Furthermore, parts of a given image often resemble other parts of the same size. The encoding algorithm based on PIFS-SF takes all this into account (Grzywna et al. 2003). It is assumed that image (texture) is a union ("collage") of its diminished, contractive and repeated copies. The transformations producing these copies deliver the list of codes for the image. The image itself is an attractor of these transformations; hence, their interactive applications to an arbitrary, initial image provides a deterministic algorithm to decode the image. Its analytical form consists of three transformations and can be presented as follows (for details see Grzywna and Stolarczyk 2002):

1. Constant value assignment:

$$\tau_1\left(\begin{bmatrix} x \\ y \\ z \end{bmatrix}\right) = \begin{bmatrix} 1 & 0 & 0 \\ 0 & 1 & 0 \\ 0 & 0 & 0 \end{bmatrix}\begin{bmatrix} x \\ y \\ z \end{bmatrix} + \begin{bmatrix} 0 \\ 0 \\ z_0 \end{bmatrix} \tag{8}$$

where z denotes the grey-level value (luminance).

2. Contractive transform:

$$\tau_2\left(\begin{bmatrix} x \\ y \\ z \end{bmatrix}\right) = \begin{bmatrix} a & b & 0 \\ c & d & 0 \\ 0 & 0 & s_z \end{bmatrix}\begin{bmatrix} x \\ y \\ z \end{bmatrix} + \begin{bmatrix} e \\ f \\ t_z \end{bmatrix} \tag{9}$$

where s_z and t_z stand for grey-level scaling. In practice, the transform is calculated as a series of simpler transforms:

$$\tau_2\left(\begin{bmatrix} x \\ y \\ z \end{bmatrix}\right) = \begin{bmatrix} 1 & 0 & 0 \\ 0 & 1 & 0 \\ 0 & 0 & s_z \end{bmatrix}\begin{bmatrix} a_1 & a_2 & 0 \\ a_3 & a_4 & 0 \\ 0 & 0 & 1 \end{bmatrix}\begin{bmatrix} s_{xy} & 0 & 0 \\ 0 & s_{xy} & 0 \\ 0 & 0 & 1 \end{bmatrix}\begin{bmatrix} x - x_D \\ y - y_D \\ z \end{bmatrix} + \begin{bmatrix} x_R \\ y_R \\ t_z \end{bmatrix} \tag{10}$$

where a_{1-4} are the coefficients of eight basic isometries (identity, reflections by mid-vertical and mid-horizontal axes, reflections by two diagonals and rotations by $+90°$, $+180$ and $-90°$); s_{xy} is the coefficient of contraction (ratio of range block size and domain block size); and (x_R, y_R) and (x_D, y_D) are the coordinates of the upper left corners of range and domain block.

3. Copying the transform:

$$\tau_3\left(\begin{bmatrix} x \\ y \\ z \end{bmatrix}\right) = \begin{bmatrix} a_1 & a_2 & 0 \\ a_3 & a_4 & 0 \\ 0 & 0 & 1 \end{bmatrix}\begin{bmatrix} x - x_D \\ y - y_D \\ z \end{bmatrix} + \begin{bmatrix} x_R \\ y_R \\ 0 \end{bmatrix} \tag{11}$$

The number of PIFS-SF codes is then equal to the total number of linear equations delivered by the above set.

Data handling

For each condition, 100–150 cells were assessed, from at least three different experiments. The mean values of D_q and number of PIFS-SF codes were determined for the cells from each dish (about 30–50 cells). These values were averaged for the three experimental repeats and the standard errors calculated. Student's t-test was used for the statistical analyses.

Results

Typical micrographs and digitized images of Mat-LyLu and AT-2 cells labelled by endocytic/vesicular uptake of HRP are shown in Figs. 1 and 2, respectively. The quantitative data obtained are summarized in Table 1.

Initial observations

Mat-LyLu and AT-2 cells were significantly different in the extent of their endocytic membrane activities when measured as the amount of HRP taken up relative to cell size (Fig. 1A, C). When uptake was performed in the presence of TTX, however, the labeling of Mat-LyLu cells was greatly reduced (Fig. 1A versus B). Details of these data concerning the *quantity* of HRP uptake and their statistical analyses were described earlier by Mycielska et al. (2003).

Patterning of staining

As well as the quantity of staining being different, it was apparent that there was a difference in the *pattern* of the labelled vesicles. On the whole, the vesicles were quite evenly distributed in the AT-2 cells, whilst Mat-LyLu cells had their staining more irregularly concentrated mainly around the nucleus and also formed larger aggregates of vacuoles (Fig. 1). The staining patterns were evaluated by the multifractal and PIFS-SF analyses. Figure 2 illustrates the basic box counting method used in the new analyses.

Multifractal analyses

The generalized fractal dimension, D_q, and the multifractal spectrum, $f(\alpha)$, for Mat-LyLu and AT-2 cells taking up HRP under control conditions and in the presence of TTX are shown in Fig. 3 (parts A and B, respectively). The value of the fractal dimension D_0

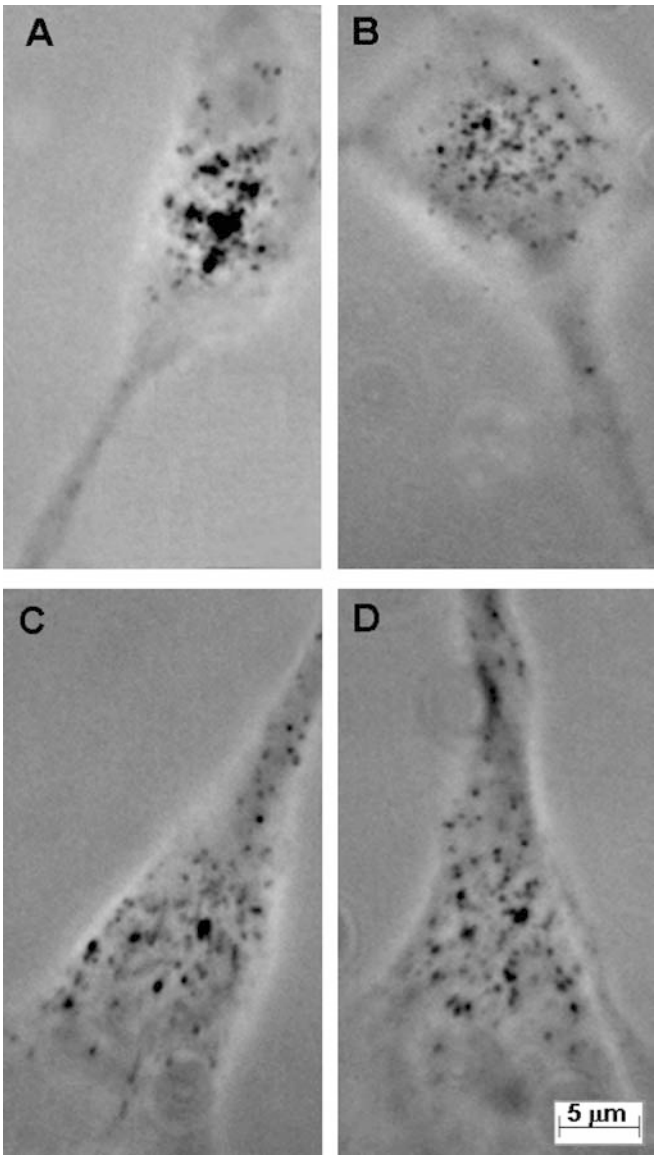

Fig. 1 Typical light micrographs of rat prostate cancer cells: Mat-LyLu (**A**, **B**) and AT-2 (**C**, **D**) showing endocytic/vesicular uptake of HRP under different conditions. **A**, **C** Controls; **B**, **D** cells pre-treated with tetrodotoxin (1 μM). In these data, "control" means uptake under normal tissue culture conditions (i.e. with no TTX present). *Scale bar* applies to all parts of the figure

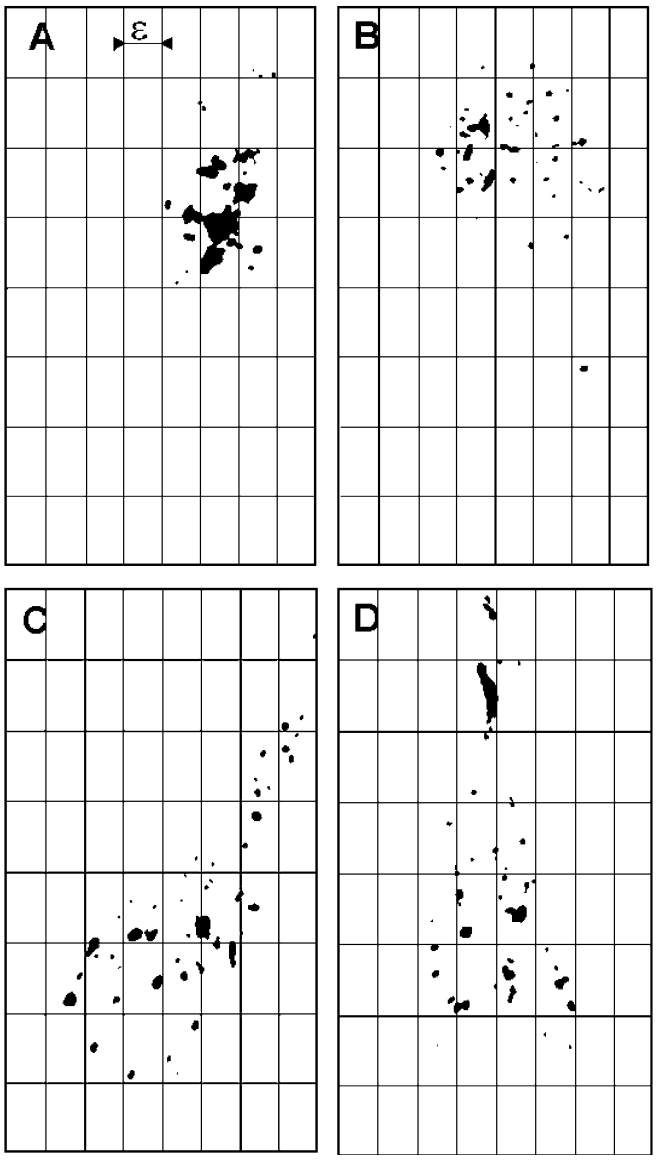

Fig. 2A–D As in Fig. 1, but showing digitized images, as required for the fractal and PIFS-SF analyses, i.e. grey-level threshold techniques provide binary images of endocytic/vesicular uptake of HRP under different conditions. **A**, **B** Mat-LyLu cells; **C**, **D** AT-2 cells. **A**, **C** Controls; **B**, **D** cells pre-treated with tetrodotoxin (1 μM). *Scale bar* applies to all parts of the figure. The figure also illustrates the box covering/counting method used for the fractal and PIFS-SF analyses of cells shown in Fig. 1. The parameter "ϵ" denotes the size of the unitary box (see text for definition)

was much higher for the Mat-LyLu compared with the AT-2 cells (1.68 ± 0.05 versus 1.43 ± 0.05; $P < 0.002$). However, in the presence of 1 μM TTX, the values of D_0 for these two cell lines became almost identical: 1.45 ± 0.05 and 1.41 ± 0.05 ($P > 0.05$), respectively (Fig. 4A; Table 1). The difference disappeared primarily due to TTX reducing the D_0 value of the Mat-LyLu cells. The values of D_1, D_2, D_{-1} and D_{-2} were also different between the two cell lines, the parameters being greater for Mat-LyLu cells in all cases (Table 1). In the case of D_1 and D_2, TTX again eliminated the difference, but this time the effect was due mainly to increasing the values for the AT-2 cells (Table 1). As regards D_{-1} and D_{-2}, in contrast, TTX pre-treatment increased the cellular differences by decreasing the values for AT-2 and increasing them for Mat-LyLu cells (Table 1).

The values of ΔD were also significantly different between the two cell lines (Table 1; Fig. 4B). TTX pre-treatment had no effect on this parameter for the AT-2 cells; however, TTX reduced it dramatically for the MAT-LyLu cells (Table 1; Fig. 4B).

Table 1 Summary of quantitative data (means ± standard errors) obtained from the different analytical approaches employed in the present study (digital imaging, and analyses of multifractals and PIFS-SF codes). All the parameters listed have been defined in the text. The data for "*E*" have been reproduced from Mycielska et al. (2003) and included here for completeness. Each data set was obtained from the measurement of 100–150 cells, from at least three different experiments

Parameter	AT-2 control	Mat-LyLu control	AT-2 with TTX	Mat-LyLu with TTX
E (%)	2.70 ± 0.20	5.40 ± 0.20	2.10 ± 0.20	2.60 ± 0.20
$D_{-\infty}$	2.45 ± 0.05	2.65 ± 0.05	2.82 ± 0.05	2.02 ± 0.05
D_{-2}	1.83 ± 0.05	2.01 ± 0.05	2.12 ± 0.05	1.69 ± 0.05
D_{-1}	1.63 ± 0.05	1.79 ± 0.05	1.89 ± 0.05	1.59 ± 0.05
D_0	1.43 ± 0.05	1.68 ± 0.05	1.41 ± 0.05	1.45 ± 0.05
D_1	1.24 ± 0.05	1.43 ± 0.05	1.40 ± 0.05	1.42 ± 0.05
D_2	1.12 ± 0.05	1.37 ± 0.05	1.40 ± 0.05	1.38 ± 0.05
D_∞	0.84 ± 0.05	1.21 ± 0.05	1.22 ± 0.05	1.24 ± 0.05
ΔD	1.62 ± 0.05	1.44 ± 0.05	1.60 ± 0.05	0.78 ± 0.05
Number of PIFS-SF codes	81 ± 20	153 ± 25	76 ± 20	51 ± 20

PIFS-SF analysis

The results of the PIFS-FS analysis are summarized in Table 1 and illustrated in Fig. 5. Under control conditions, the number of codes ($N_{\text{PIFS-SF}}$) was much higher for the MAT-LyLu (153 ± 25) compared with AT-2 cells (81 ± 20) ($P < 0.003$). Pre-treatment with TTX had no effect on the AT-2 cells, whilst there was a significant reduction in the value for the MAT-LyLu cells (Table 1; Fig. 5).

Discussion

The main conclusions of the present study are as follows:

1. The quantity and quality (pattern) of the vesicular staining were different between the two cell lines. Under control conditions, all multifractal and PIFS-SF parameters determined had values greater for Mat-LyLu compared with AT-2 cells. These data taken together would be in general agreement with the endocytic/vesicular activity of the strongly metastatic Mat-LyLu cells being more developed than the corresponding weakly metastatic AT-2 cells. We have shown previously that the same is true for the quantity of the staining, as represented by the parameter "*E*" (Mycielska et al. 2003).
2. Some of the parameters (E, D_0, $N_{\text{PIFS-SF}}$) had a "simple" dependence on VGSC activity, whereby pre-treatment with TTX reduced the values for the MAT-LyLu cells and eliminated the differences between the two cell lines.

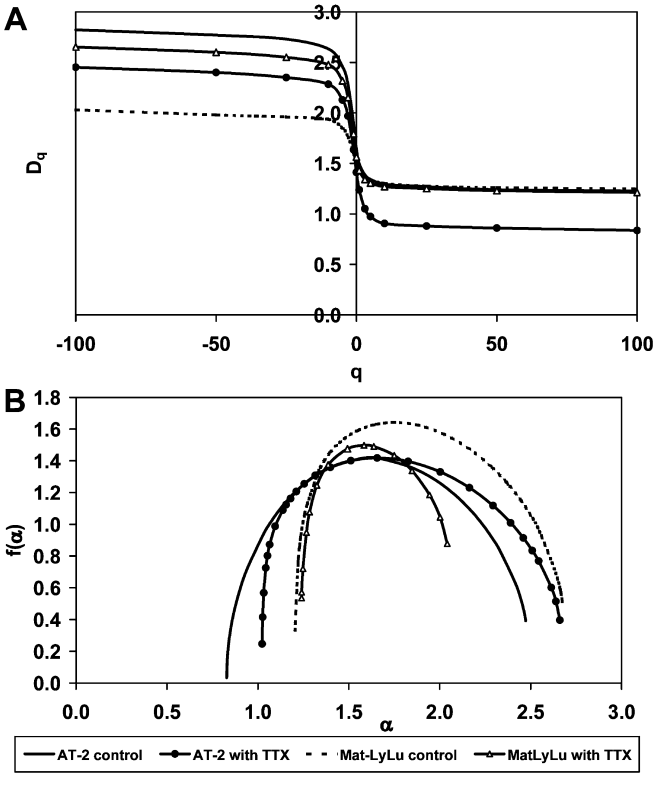

Fig. 3 Averaged profiles of the generalized fractal dimension D_q (**A**) and the $f(\alpha)$ spectrum (**B**) for Mat-LyLu and AT2 cells under control and 1 μM TTX pre-treated conditions (specified by the *key at the bottom*)

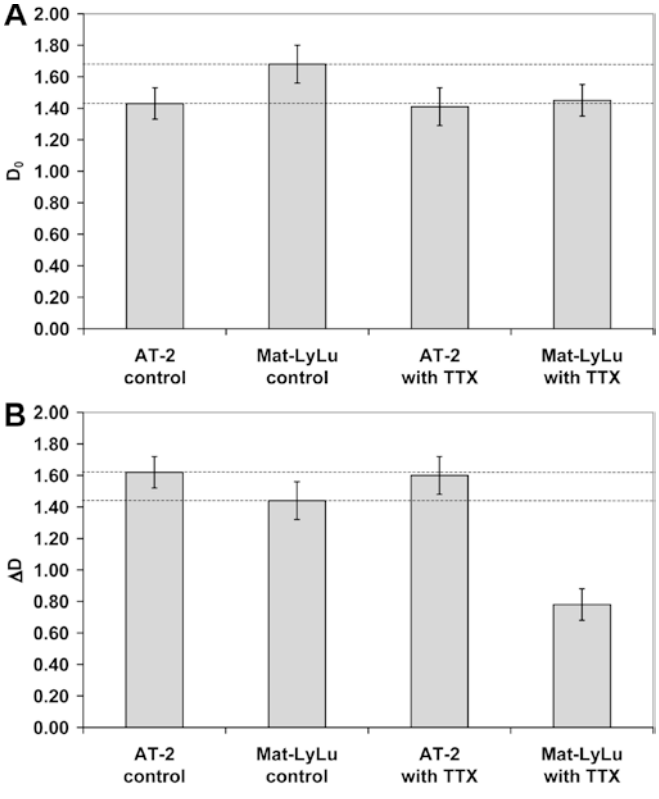

Fig. 4 Values of the parameters ΔD [width of $f(\alpha)$ spectrum, i.e. difference between D_∞ and $D_{-\infty}$] (**A**) and the fractal dimension D_0 (**B**) determined for Mat-LyLu and AT-2 cells under control and 1 μM TTX pre-treated conditions. Each *histobar* denotes the mean ± standard error. The *dotted horizontal lines* indicate the control levels for comparison

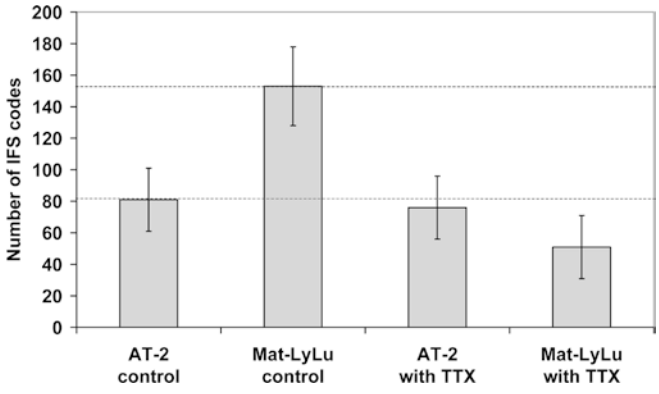

Fig. 5 The numbers of PIFS-SF codes determined for Mat-LyLu and AT-2 cells under control and 1 μM TTX pre-treated conditions. Each *histobar* denotes the mean ± standard error. The *dotted horizontal lines* indicate the control levels for comparison

3. All the other parameters (D_1, D_2, D_{-1}, D_{-2} and ΔD) were also sensitive to TTX but the dependences were more "complex".

Control of endocytic vesicles by VGSC activity

"Simple" parameters: E, D_0, $N_{PIFS\text{-}SF}$

We have shown earlier that the parameter "*E*" quantified the amount of tracer uptake relative to cell size and revealed that the MAT-LyLu cells were more endocytic than the AT-2 cells, in line with the much stronger metastatic character of the former (Mycielska et al. 2003). TTX suppressed substantially the extent of HRP uptake into the MAT-LyLu cells, consistent with the expression of functional VGSCs in these cells (Grimes et al. 1995). The parameter D_0 ("fractal dimension") scales aggregation of mass with distance from the centre and can be viewed as complementary to *E*. Indeed, just as in the case of *E*, the value of D_0 was greater for MAT-LyLu compared with AT-2 cells and TTX eliminated this difference. The number of PIFS-SF codes, which would also depend on the "weight" of staining, showed the same tendency, i.e. the larger the mass of staining and its spatial heterogeneity within the cell, the higher the PIFS-SF codes. Thus, VGSC activity would enhance metastatic potential by potentiating all three aspects representing the quantity and complexity of endocytosis.

The possible ways of VGSCs involvement in the endocytic process have already been discussed in our previous paper (Mycielska et al. 2003). Briefly, Na^+ could increase intracellular Ca^{2+} levels and thus activate protein kinase C and/or CaM kinase II and lead to phosphorylation of the actin cytoskeleton, thereby allowing secretion and endocytosis to occur (Minami et al. 1998; Gromada et al. 1999; Song et al. 1999; Trifaro et al. 2000). Furthermore, there could be a direct action of Na^+ on adenylate cyclase that could alter levels of cAMP, activate protein kinase A and, in turn, phosphorylate some component(s) of the vesicular machinery (Renstrom et al. 1996; Lee and Tse 1997; Murakami et al. 1998; Hilfiker et al. 2001). Another possibility is a direct interaction between the VGSC and some component(s) of the secretory apparatus (Sampo et al. 2000; Herzog et al. 2003).

"Complex" parameters: D_1, D_2, D_{-1}, D_{-2}, ΔD

D_1 and D_2 are the "information" and "correlation" dimensions, respectively. The latter also represents "relative tendency for aggregation" within the vesicular populations (Grzywna et al. 2001). Under control conditions, their values were significantly smaller for AT-2 compared with Mat-LyLu cells. After blocking the activity of VGSC, however, D_1 and D_2 became similar in both cell lines and close to the value for Mat-LyLu under control conditions (Table 1). Significantly different values of information and correlation dimensions for both cell lines under control conditions may be the result of different mutual interdependence within the vesicle populations in both cell lines. Strongly metastatic cells are more motile and capable of more complex signaling and behaviour, compared with the weakly metastatic AT-2 cells, where this activity is less expressed. After blocking VGSCs, which influenced the quality and location of staining, we observed, in the weakly metastatic cells, a surprising increase of values of D_1 and D_2 which reached the levels of the strongly metastatic cells. This would suggest that the cell/system, after losing one way of "processing" information, i.e. via VGSC activity, may "restructure" itself to enhance and improve in other ways (e.g. by more regularity in vesicular activity). There are also two possible implications of this result. (1) The low level of VGSC activity that may exist in AT-2 cells (Diss et al. 2001) may have a functional role. This situation would be analogous to glial cells that express a very low level of VGSC just to "energize" the Na^+/K^+-ATPase (Philippe et al. 2002). (2) The relationship between VGSC expression/activity and endocytosis may not exactly be the same in the two cell lines. A comparable situation concerning the relationship between voltage-gated K^+ channel activity and proliferation was found earlier for Mat-LyLu and AT-2 cells (Fraser et al. 2000).

The parameters D_{-1} and D_{-2} are more difficult to evaluate owing to their uncertain "physical" meaning. Nevertheless, on the whole, these parameters showed tendencies opposite to D_1 and D_2, consistent with their generally "antagonistic" nature.

As regards ΔD, which is the difference between D_∞ and $D_{-\infty}$, we can use it as a measure of the "self similarity" or the degree of aggregation of vesicles within a cell. Under control conditions, the value of this parameter was smaller for AT-2 compared with Mat-LyLu cells, consistent with the more complex staining pattern of the latter. After blocking VGSCs, ΔD was reduced to almost 50% of the control, i.e. the self-similarity increased. Although ΔD was clearly sensitive to TTX,

the relationship between VGSC activity and self-similarity of Mat-LyLu cells again appeared not straightforward. Such complexity overall may reflect the intricate nature of the endocytic machinery that one would expect to operate in a strongly metastatic/secretory cell line.

Conclusions

In conclusion, first, multifractal as well as PIFS-SF methods would appear overall to be highly suitable for quantitative analyses of the amount and pattern of endocytic vesicles in cancer cells. Second, it is clear that VGSC activity controls both aspects of the endocytic process, consistent with its previously proposed role as an accelerating factor in prostate cancer metastasis (Djamgoz 2001). Further work remains to be done, however: (1) to elucidate the nature of the VGSC control of endocytosis in a wider range of strongly versus weakly metastatic cell lines, in both "'quantitative'' and ''qualitative'' respects, including the correlation with fractals and PIFS-SF codes; (2) to determine the precise physical/physiological meaning of the parameters; and (3) to extend this understanding to specific secretions and associated cell behaviour.

Acknowledgements This study was supported by the Pro Cancer Research Fund (PCRF), and collaboration grants from NATO (Scientific Division) and the British Council (Warsaw). Z.J.G. would like to acknowledge the generous hospitality of Ealing Abbey during stays in London.

References

Almqvist N (1996) Fractal analysis of scanning probe microscopy images. Surf Sci 355:221–228

Barnsley M (1988) Fractals everywhere. Academic Press, New York

Bashyam MD (2002) Understanding cancer metastasis: an urgent need for using differential gene expression analysis. Cancer 94:1821–1829

Bottino DA, Kleen M, Kemming G, Meisner F, Habler O, Messmer K (2001) Three-dimensional visualization of lung blood flow heterogeneity based on fluorescent microsphere technique and fractal dimension: the blood flow analysis system – BFA system. Comput Methods Programs Biomed 65:79–87

Conner SD, Schmid SL (2003) Regulated portals of entry into the cell. Nature 422:37–44

Diss JKJ, Archer SN, Hirano J, Fraser SP, Djamgoz MBA (2001) Expression profiles of voltage-gated Na(+) channel alpha-subunit genes in rat and human prostate cancer cell lines. Prostate 48:165–178

Djamgoz MBA (2001) Excitability of prostate cancer cells: a new concept in the pathophysiology of metastatic disease. Br J Cancer 85(suppl 1):8

Djamgoz MBA, Krasowska M, Martinoli O, Sericano M, Vallerga S, Grzywna ZJ (2001) Structure–function correlation in transient amacrine cells of goldfish retina: basic and multifractal analyses of dendritic trees in distinct synaptic layers. J Neurosci Res 66:1208–1216

Evans CP, Walsh DS, Kohn EC (1991) An autocrine motility factor secreted by the Dunning R-3327 rat prostatic adenocarcinoma cell subtype AT2.1. Int J Cancer 49:109–113

Foster CS, Cornford P, Forsyth L, Djamgoz MBA, Ke Y (1999) The cellular and molecular basis of prostate cancer. Br J Urol Int 83:171–194

Fraser SP, Grimes JA, Djamgoz MBA (2000) Effects of voltage-gated ion channel modulators on rat prostatic cancer cell proliferation: comparison of strongly and weakly metastatic cell lines. Prostate 44: 61–76

Grimes JA, Fraser SP, Stephens GJ, Downing JE, Laniado ME, Foster CS, Abel PD, Djamgoz MBA (1995) Differential expression of voltage-activated Na^+ currents in two prostatic tumour cell lines: contribution to invasiveness in vitro. FEBS Lett 369:290–294

Gromada J, Hoy M, Renstrom E, Bokvist K, Eliasson L, Gopel S, Rorsman P (1999) CaM kinase II-dependent mobilization of secretory granules underlies acetylcholine-induced stimulation of exocytosis in mouse pancreatic B-cells. J Physiol (London) 518:745–759

Grzywna ZJ, Stolarczyk J (2002) On some structure-morphology problems by the extended partioned iterated function system (PIFS-SF). Chaos Solitons Fractals 13:897–905

Grzywna ZJ, Krasowska M, Ostrowski , Stolarczyk J (2001) Can generalized dimension (D_q) and $f(\alpha)$ be used in structure–morphology analysis? Acta Phys Polon B 32:1561–1577

Grzywna ZJ, Krasowska M, Stolarczyk J (2003) On the application of PIFS-SF and D_q ($f(\alpha)$) to dendrites analysis. Acta Phys Polon B 34:3681–3693

Gundelfinger ED, Kessels MM, Qualmann B (2003) Temporal and spatial coordination of exocytosis and endocytosis. Nat Rev Mol Cell Biol 4:127–139

Herzog RI, Liu C, Waxman SG, Cummins TR (2003) Calmodulin binds to the C terminus of sodium channels Nav1.4 and Nav1.6 and differentially modulates their functional properties. J Neurosci 23:8261–8270

Hilfiker S, Czernik AJ, Greengard P, Augustine GJ (2001) Tonically active protein kinase A regulates neurotransmitter release at the squid giant synapse. J Physiol (London) 531:141-146

Isaacs JT, Isaacs WB, Feitz WF, Scheres J (1986) Establishment and characterization of seven Dunning rat prostatic cancer cell lines and their use in developing method for predicting metastatic abilities of prostatic cancers. Prostate 9:261–281

Jaquin AE (1993) Fractal image coding – a review. Proc IEEE 81:1451–1465

Jelinek HF, Fernandez E (1998) Neurons and fractals: how reliable and useful are calculations of fractal dimension? J Neurosci Methods 81:9-18

Kurbel S, Kurbel B, Kovacic D, Sulava D, Krajina Z, Dimitrovic B, Sokcevic M (1999) Endothelin-secreting tumors and the idea of the pseudoectopic hormone secretion in tumors. Med Hypoth 52:329–233

Laniado ME, Lalani E-N, Fraser SP, Grimes JA, Bhangal G, Djamgoz MBA, Abel PD (1997) Expression and functional analysis of voltage-activated Na^+ channels in human prostate cancer cell lines and their contribution to invasion in vitro. Am J Pathol 150:1213–1221

Latka M, Glaubic-Latka M, Latka D, West BJ (2004) Fractal rigidity in migraine. Chaos Solitons Fractals 20:165–170

Lasota A, Myjak J (1996) Semifractals. Bull Pol Acad Sci Math 44:5–21

Lee AK, Tse A (1997) Mechanism underlying corticotropin-releasing hormone (CRH) triggered cytosolic Ca^{2+} rise in identified rat corticotrophs. J Physiol (London) 504:367–378

Lin SW, Lee MT, Ke FC, Lee PP, Huang CJ, Ip MM, Chen L, Hwang JJ (2000) TGFbeta1 stimulates the secretion of matrix metalloproteinase 2 (MMP2) and the invasive behavior in human ovarian cancer cells, which is suppressed by MMP inhibitor BB3103. Clin Exp Metastasis 18:493–439

Liotta LA (1986) Molecular biology of metastases: a review of recent approaches. Eur J Cancer Clin Oncol 22:345–348

Llorente A, van Deurs B, Garred O, Eker P, Sandvig K (2000) Apical endocytosis of ricin in MDCK cells is regulated by the cyclooxygenase pathway. J Cell Sci 113:1213–1221

Minami N, Berglund K, Sakaba T, Kohmoto H, Tachibana M (1998) Potentiation of transmitter release by protein kinase C in goldfish retinal bipolar cells. J Physiol (London) 512:219–225

Murakami Y, Tanaka J, Koshimura K, Kato Y (1998) Involvement of tetrodoxin-sensitive sodium channels in rat growth hormone secretion induced by pituitary adenylate cyclase-activating polypeptide (PACAP). Regul Pept 73:119–121

Mycielska ME, Szatkowski M, Djamgoz MBA (2003) Contribution of functional voltage-gated Na^+ channel expression to cell behaviours in the matastatic cascade in rat prostate cancer. II. Secretory membrane activity. J Cell Physiol 195:461–469

Nicholson B, Schaefer G, Theodorescu D (2001) Angiogenesis in prostate cancer: biology and therapeutic opportunities. Cancer Metastasis Rev 20:297–319

Philippe JM, Dubois JM, Rouzaire-Dubois B, Cartron PF, Vallette F, Morel N (2002) Functional expression of V-ATPases in the plasma membrane of glial cells. Glia 37:365–373

Renstrom E, Eliasson L, Bokvist K, Rorsman P (1996) Cooling inhibits exocytosis in single mouse pancreatic B-cells by suppression of granule mobilization J Physiol (London) 494:41–52

Sampo B, Tricaud N, Leveque C, Seagar M, Couraud F, Dargent B (2000) Direct interaction between synaptotagamin and intracellular loop I–II of neuronal voltage-gated sodium channels. Proc Natl Acad Sci USA 28:3666–3671

Schroeder M (1991) Fractals, chaos, power laws. Freeman, New York

Shtiegman K, Yarden Y (2003) The role of ubiquitylation in signaling by growth factors: implications to cancer. Semin Cancer Biol 13:29–40

Siwy Z, Mycielska M, Djamgoz MBA (2003) Statistical and fractal analyses of rat prostate cancer cell motility in direct-current electric field: comparison of strongly and weakly metastatic cells. Eur Biophys J 32:12–21

Song JC, Hrnjez BJ, Farokhzad OC, Matthews JB (1999) PKC-epsilon regulates basolateral endocytosis in human T84 intestinal epithelia: role of F-actin and MARCKS. Am J Physiol 277:C1239–C1249

Stanley HG (1996) Fractals and multifractals: the interplay of physics and geometry. In: Bunde A, Havlin S (eds) Fractals and disordered systems. Springer, Berlin Heidelberg New York

Trifaro J, Rose SD, Lejen T, Elzagallaai A (2000) Two pathways control chromaffin cell cortical F-actin dynamics during exocytosis. Biochimie 82:339–352

Turiel A (2003) Relevance of multifractal textures in static images. Electron Lett Comput Vision Image Anal 1:35–49

Vico PG, Boyer H, Carlier LH (1994) New concept in the study of tissue vascularization. Plast Reconstr Surg 94:174–179

Yang PC, Berin MC, Yu LC, Conrad DH, Perdue MH (2000) Enhanced intestinal transepithelial antigen transport in allergic rats is mediated by IgE and CD23 (FcepsilonRII). J Clin Invest 106:879–886